Effect of loading type on the fatigue strength of asymmetric and symmetric transverse non-load carrying attachments

A. Ahola*, T. Nykänen, T. Björk
School of Energy Systems, Lappeenranta University of Technology, P.O. Box 20, FI-53851 Lappeenranta, Finland

ABSTRACT

This study considers the effect of bending loading and the symmetry of joints on the fatigue strength of transverse non-load carrying attachments. Conventionally, the fatigue strength of a welded joint has been determined without taking these factors into account. Experimental and finite element analyses (FEAs) were carried out and both methods showed that both loading type and symmetry have an influence on the fatigue resistance of a welded joint. Under tensile loading, the fatigue strength of asymmetric T-joints was higher than that of symmetric X-joints. Respectively, the fatigue resistance of tested joints improved explicitly when the external loading was bending. The FEA was in good agreement with the test results in the joints subjected to tension but gave very conservative results in the joints subjected to bending.

Keywords: fatigue, welded joints, loading type, symmetry of joint, fatigue assessment approaches

NOMENCLATURE

2D	two-dimensional
ASW	as-welded
CVN	Charpy V-notch
DNV-GL	Det Norske Veritas - Germanischer Lloyd
DOB	degree of bending
ENS	effective notch stress
FAT	fatigue strength, stress range corresponding to two million cycles
FEA	Finite element analysis
GMAW	gas metal arc welding
HS	hot spot
IIW	International Institute of Welding
LEFM	linear elastic fracture mechanics
LSE	linear surface extrapolation
MC	thermo-mechanically treated steel
SCF	stress concentration factor
TTWT	through thickness at weld toe
A_5	uniform elongation
C	crack propagation coefficient
C_f	fatigue capacity
E	elastic modulus
f_u	ultimate strength
f_y	yield strength
I	current

*Correspondence: A. Ahola, E-mail: antti.ahola@lut.fi

k_f	effective stress concentration factor
k_m	structural stress concentration factor for misalignment
k_t	stress concentration factor
l	half of distance between clamps
m	slope of *S-N* curve or Paris' law
N_{cp}	crack propagation time
N_f	fatigue life
N_i	crack initiation time
Q	heat input
R	applied stress ratio
Stdv	standard deviation
t	plate thickness
$t_{8/5}$	cooling rate (800°C–500°C)
q_{geom}	fatigue strength ratio for symmetry type
q_{load}	fatigue strength ratio for loading type
v	travel speed
v_{wire}	wire feed rate
U	voltage
α	angular misalignment
Δ	range
ρ	actual notch radius
θ	flank angle
σ	stress

INDICES

asym	asymmetric T-joint
b	bending
char	characteristic value
m	membrane
max	maximum
mean	mean value
nom	nominal
res	residual stress
SG	strain gage measurement value
SL	shape laser measurement value
sym	symmetric X-joint

INTRODUCTION

The *S-N* curves used in the stress based fatigue assessment approaches for welded joints, i.a. nominal stress, hot spot (HS) stress and effective notch stress (ENS) methods, are typically determined by means of fatigue tested joints and structures subjected to tension[1–3], and therefore, bending stress occurs only as a secondary component. The current recommendations and codes[4–6] do not have consistent specifications how the degree of bending (DOB, bending stress divided by maximum stress) in the external loading or in the HS stress components should be taken into account. The conventional concept has been that only the maximum stress range is evaluated regardless of the DOB. Additionally, the symmetry of the joint, i.e. whether the attachment is one-sided or double-sided, Fig. 1, is also neglected.

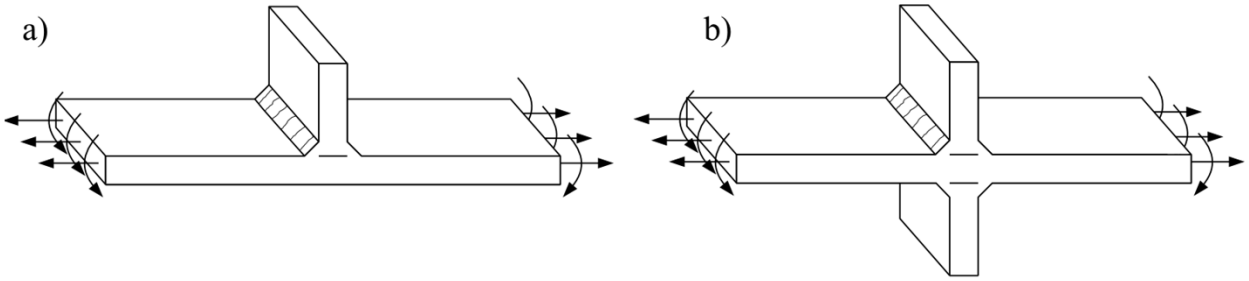

Fig. 1 Two types of symmetry in non-load carrying joints: (a) asymmetric T-joint and (b) symmetric X-joint with fillet welds under tensile and bending loading.

However, several studies have shown that the stress concentration factors (SCF) of non-load carrying joints depend highly on both the DOB and the symmetry of the joint. For instance, Japanese research institutes have demonstrated that the notch effect is higher when the DOB increases if the joint is asymmetric.[7] Respectively, membrane stress causes a greater notch effect when the joint is symmetric compared to the corresponding asymmetric joint, which can be discovered also from the stress magnification factors M_k determined by Lie *et al.*[8]. Additionally, fatigue test results have indicated an improvement of fatigue strength in asymmetric joints subjected to tension and in symmetric joints subjected to bending.[9, 10] This might lead to problematic design issues in the assessment of fatigue life if it is done by using a nominal or HS stress method since the codes give only one fatigue strength (FAT) for each type of joint despite the DOB or symmetry of the joint.

Another aspect in bending loading relates to the stress gradient through the thickness. In the early phase of crack propagation, the decreasing stress distribution through thickness under bending results in the stress and stress intensity factor (SIF) being lower at the crack tip. Consequently, the crack propagation rate decreases and fatigue strength improves. This rationalizes why Det Norske Veritas - Germanischer Lloyd (DNV-GL) allows a 40% reduction for the bending stress component in the evaluation of equivalent HS stress. On the other hand, DNV-GL justifies the use of the reduction by the redistribution of loads when a crack propagates. In that case, the reduction factor can be utilized, according to DNV-GL, if the stress is highly localized and the crack development rather displays displacement controlled behavior instead of load controlled behavior. Additionally, the reduction factor is applicable only if crack propagation is allowed in the structure, and hence, the redistribution of loads occurs.[6, 11]

British Standards included a correction factor of the DOB and plate thickness in the revision of BS7608:1993, which was explained by fracture mechanics based calculations. The factor enhances the fatigue strength of welded joints when the DOB increases. Maddox[1] re-estimated the effect of bending, leaning on the existing test data of both load carrying and non-load carrying joints, and drew the conclusion that fracture mechanics overestimates, compared to the test results, the beneficial effect of bending. In most of the reviewed studies, the conclusion was that the increasing DOB improves the fatigue strength of welded joints, but Ottersböck *et al.*[12] presented an entirely opposite point of view. Ottersböck *et al.* conducted fatigue tests for non-load carrying T-joints subjected to tensile and bending loads. The bending test results expressed a loss of fatigue strength in terms of the nominal stress method compared to tensile loaded joints in as-welded (ASW) conditions. The results have reasonable agreement with the ENS method since higher SCFs were obtained for the bending loaded joints.

Generally, in previous studies, comparisons have been made by using the nominal stress system. The effect of the loading type is sensitive to structural imperfections since e.g. an angular distortion produces a secondary bending stress component and increases the structural stress when the external loading is axial. Respectively, if the external loading is pure bending (DOB = 1), angular distortion does not increase the structural stress. This aspect needs to be considered when the magnitude of the effect is evaluated with the nominal stress system. In this study, the effect of the loading type and symmetry was investigated by means of experimental tests and FEA. The following fatigue strength ratios were established to compare the fatigue strength of asymmetric T-joints (FAT_{asym}) and symmetric X-joints (FAT_{sym}) as well as tensile and bending loading:

$$q_{geom} = \frac{FAT_{asym}}{FAT_{sym}} \tag{1}$$

$$q_{load} = \frac{FAT_{m}}{FAT_{b}} \tag{2}$$

In Eq. (2) FAT_m is the fatigue strength for tensile loaded joints and FAT_b for bending loaded joints, respectively. Fatigue tests were carried out for asymmetric and symmetric transverse attachment joints subjected to tension and pure bending. In the fatigue assessment, both stress based methods and linear elastic fracture mechanics (LEFM) were considered, and the analyses were carried out for two-dimensional (2D) plane strain element models.

FATIGUE TESTS

Test specimens

A total of 12 non-load carrying transverse attachment joints were manufactured to examine the effect of the DOB and joint symmetry on the fatigue strength of non-load carrying joints. The specimens were fabricated from SSAB's product S960 MC, ultra-high strength steel (UHSS) plates with a plate thickness of t = 8 mm by using a gas metal arc welding (GMAW) process (135) and welding robot, Fig 2. The fillet welds were produced by using a single-pass welding. Between the passes, the specimen was allowed to cool down to room temperature. Consequently, the uniformity of metallurgical welding quality in the test series could be ensured. Weld run-on and run-off parts were removed and the edges of the specimens were ground to avoid crack initiation and propagation from the edge of the sheet. Six specimens of both symmetry types, i.e. asymmetric T-joints and symmetric X-joints, were fabricated. The mechanical properties and chemical compositions of the materials used are presented in Table 1 and the welding parameters in Table 2.

Table 1 Mechanical properties and chemical compositions of the base and filler material used in the fatigue tests. f_y is yield strength, f_u ultimate strength, A_5 uniform elongation and CVN Charpy V-notch impact energy.

Mechanical properties												
Material	f_y [MPa]			f_u [MPa]			A_5 [%]			CVN [J]		
S960 MC	960			980-1250			7			27		
Union X96	930			980			14			47		
Chemical compositions [weight-%]												
Material	C	Si	Mn	P	S	Al_{tot}	Nb	V	Ti	Cr	Mo	Ni
S960 MC	0.12	0.25	1.u3	0.02	0.01	0.015	0.05	0.05	0.07	-	-	-
Union X96	0.12	0.8	1.9	-	-	-	-	-	-	0.45	0.55	2.35

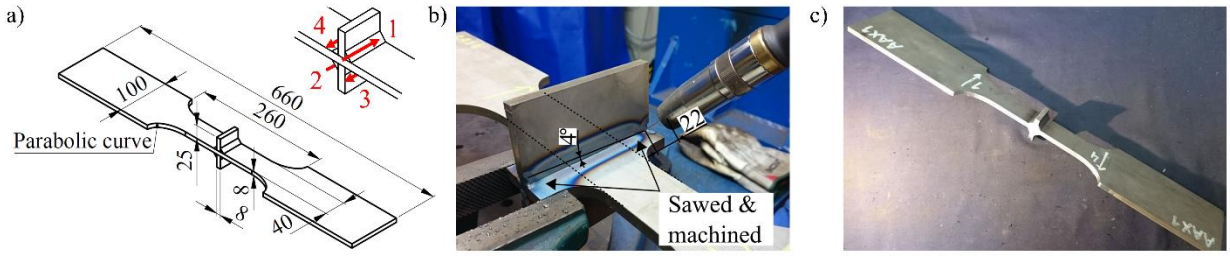

Fig. 2 (a) Dimensions of the X-joint case and sequence of welds, (b) welding procedure and (c) a fabricated specimen. The dimensions of the T-joint specimens are identical but the attachment is one-sided and the sequence of welds corresponds to the pass numbers 1 and 4.

Table 2 Average values of welding parameters.

	Current I [A]	Voltage U [V]	Travel speed* v [mm/s]	Wire feed speed* v_{wire} [m/min]	Heat input Q [kJ/mm]	Cooling rate $t_{8/5}$ [s]
Average	229.6	28.8	5.9	13.2	0.90	7.4
Standard deviation (Stdv)	1.9	0.1	-	-	0.007	0.1

*Constant value

The global shape and weld geometry of the specimens were measured from the finished specimen by applying shape laser measurements. In the T-joints, the angular distortion was significantly higher compared to the corresponding X-joints because the heat input was directed only to one side of the base plate and the deformation of the specimens was not prevented, Fig. 2b. When fixed end constraints are applied and the straightening of the specimen due to membrane loading is taken into account, the structural stress concentration factor for misalignment, k_m, can be estimated by using the following equation[4]:

$$k_m = 1 + \frac{3 \bullet \alpha \bullet l}{2t} \quad \frac{\tanh \frac{\beta}{2}}{\frac{\beta}{2}}, \tag{3}$$

where

$$\beta = \frac{2l}{t} \cdot \sqrt{\frac{3\sigma_m}{E}}. \tag{4}$$

In Eq. (3), α is angular misalignment, l half of distance between clamps. In Eq. (4), σ_m is membrane stress and E elastic modulus. These equations are valid for straight plates and the straightening due to the clamping of specimen to the test rig must be taken account separately. Shape laser measurements showed that the nominal throat thicknesses[13] were nearly identical with a_{mean} = 5.2 mm (Stdv = 0.16 mm). The measured actual notch radii ρ on the centerline of the specimens varied between 0.2 mm and 0.4 mm. Fig. 3 depicts relatively low values of the weld penetration in the T- and X-joint specimens and the evaluated values have reasonable accordance with nominal throat thicknesses evaluated by a shape laser. No post-weld treatments were performed, but the joints were in ASW condition.

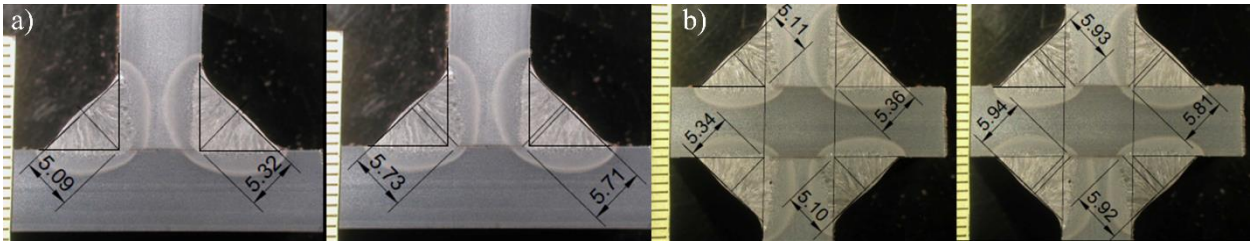

Fig. 3 Polished sections: the nominal and effective throat thicknesses[13] of (a) T-joint and (b) X-joint specimens.

The residual stresses σ_{res} were measured by using an X-ray diffractometer. The measurements were conducted at the weld toes of each specimen, and surface distribution along the specimen was measured on the centerline of a sheet for one T-joint and one X-joint, Fig. 4. The measured compressive residual stresses were relatively low, typically 0.1-0.2 · f_y, and no characteristics of the joint type could be found.

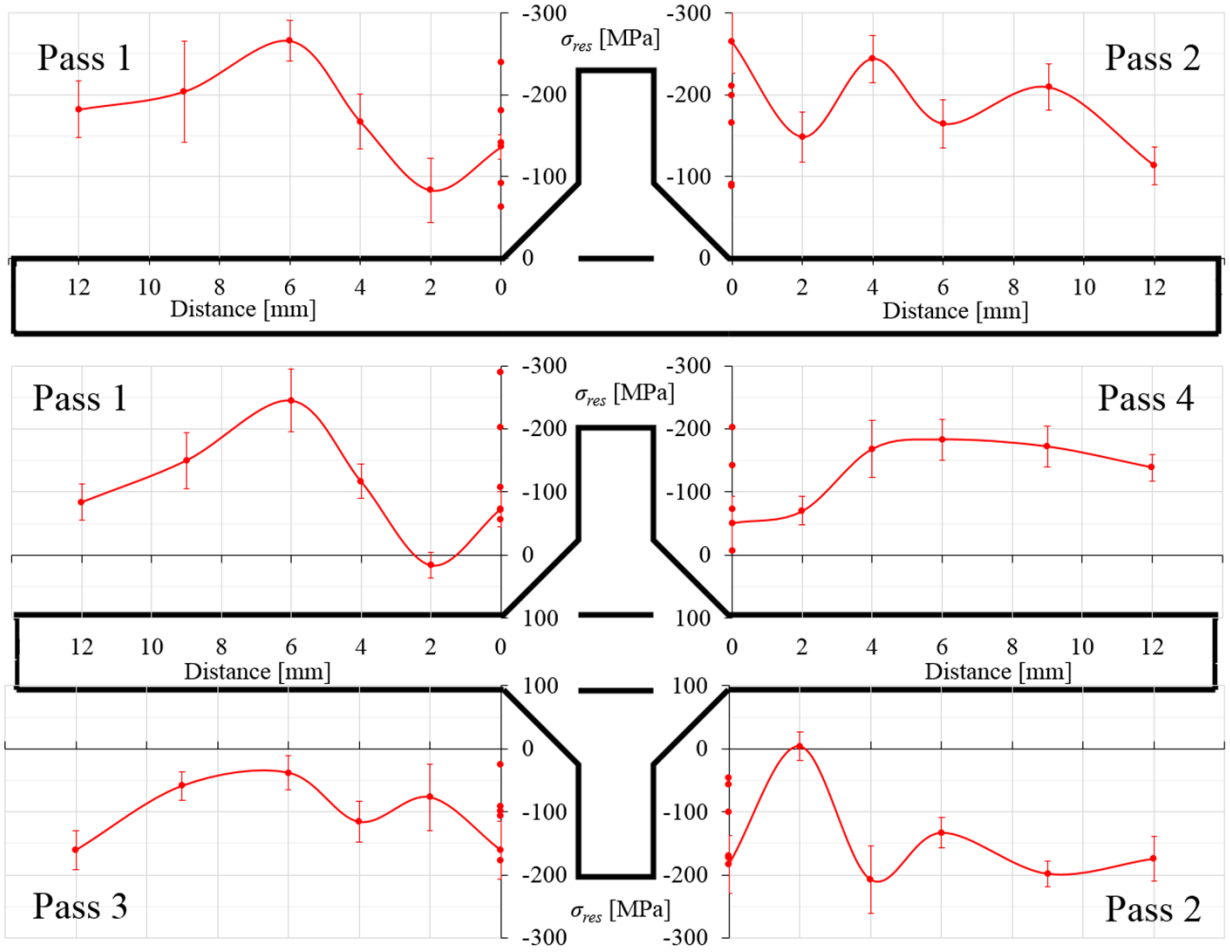

Fig. 4 Residual stress distribution along specimens and single data points at the weld toes.

Test set-up

For the fatigue tests, two types of test set-ups were applied: tensile and pure bending loading by using four-point bending when a constant moment area exists between the inner press rolls, Fig. 5b. In both test set-ups, the force was produced by the hydraulic actuator which was equipped with a force transducer to measure the minimum and maximum external fluctuating loading. For each test, a strain gage was positioned at a 0.4*t* distance from weld toe to assess the HS stress. To evaluate the HS stress more precisely, two strain gages positioned at 1.0*t* and 0.4*t* would be required to apply the linear extrapolation.[14] Still, one strain gage gives a reasonable estimation of the HS stress as shown in the next Section, Table 5. Eight specimens were subjected to bending (four T-joints and four X-joints), and the remaining four specimens were subjected to tension.

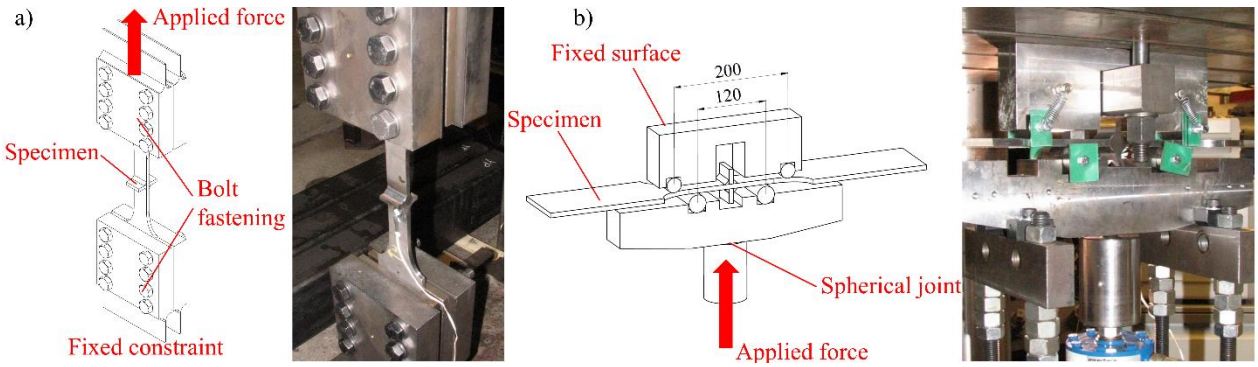

Fig. 5 Test set-ups: (a) tensile and (b) bending loading.

Results

Fatigue test data for twelve fatigue loaded transverse attachment joints are presented in Table 3. Failure criterion for the end of test was a fracture of specimen. The fracture surfaces are presented in Fig. 8. As predicted, when external loading is pure bending, DOB = 1, angular distortions did not attract a secondary bending stress component, and a concentration factor of $k_{m,SG}$ = 1.0 was received for both symmetry types. Similar behavior can be seen in the tensile loaded X-joints in which secondary bending stress did not exist since angular distortions were effectively non-existent. In the tensile loaded T-joints, in contrast, secondary bending stresses occurred. However, k_m factors evaluated by using Eq. (1) were clearly higher than k_m factors determined by strain gage measurements

although the extrapolation was neglected. This can be explained by the straightening of the specimen when it was clamped to the test rig. The straightening of the specimen was not directly measured, but the induced stress at the strain gage was identified and taken into account in true applied stress ratio, R_{true}.

Table 3 Fatigue test data. $\Delta\sigma_{nom}$ is nominal stress range, N_f fatigue life (total), N_i crack initiation time and N_{cp} crack propagation time. Indices SL and SG signify values evaluated by means of a shape laser and strain gage measurements, respectively.

ID	Joint type	Load type	$\Delta\sigma_{nom}$ [MPa]	R_{true} [-]	N_f [10^3]	N_i [10^3]	N_{cp} [10^3]	α_{SL} [10^{-3} rad]	$k_{m,SL}$ [-]	$k_{m,SG}$ [-]
AAT1	T-joint	Bending	273	0.11	886	516	370	23.8	-	1.0
AAT2	T-joint	Bending	378	0.10	172	82	90	19.5	-	1.0
AAT3	T-joint	Bending	378	0.10	166	86	80	25.2	-	1.0
AAT4	T-joint	Bending	302	0.11	476	306	170	22.8	-	1.0
AAT5	T-joint	Tension	299	0.20	94	42	52	20.0	1.36	1.26
AAT6	T-joint	Tension	210	0.26	400	320	80	24.2	1.47	1.35
AAX1	X-joint	Bending	275	0.09	500	260	240	5.1	-	1.0
AAX2	X-joint	Bending	378	0.11	138	68	70	3.7	-	1.0
AAX3	X-joint	Bending	378	0.09	125	35	95	4.6	-	1.0
AAX4	X-joint	Bending	307	0.11	378	228	150	0.8	-	1.0
AAX5	X-joint	Tension	378	0.19	37	21	16	5.7	1.10	1.00
AAX6	X-joint	Tension	248	0.07	244	184	60	3.1	1.06	1.01

S-N curves were determined by using a standard procedure based on the linear regression analysis of Eq. (5). The number of the test specimens was rather low and thus, the conducted *S-N* curves can only be used for the comparison of test results instead of determining the precise fatigue strengths of these joints.

$$\log N_f = \log C_f - m \bullet \log \Delta\sigma , \tag{5}$$

where N_f is fatigue life in cycles, C_f the fatigue capacity, m the slope of *S-N* curve and $\Delta\sigma$ the normal stress range. Curve fittings were carried out by applying both recommended[4] fixed m = 3 and free m *S-N* curve slopes. In the nominal stress system, the fatigue strength of asymmetric T-joints and symmetric X-joints under tension loading are roughly identical, Fig. 6a. Nevertheless, it must be noticed that according to strain gage measurements, the angular distortions led to $k_{m,SG}$ = 1.26 and $k_{m,SG}$ = 1.35 in the T-joints. In the X-joints, the angular distortions were minor and there was no secondary bending component. Thus, nominal stresses were equal to HS stresses. According to International Institute of Welding (IIW)[4], the nominal stress system covers only misalignments leading to $k_{m,max}$ = 1.3. Consequently, the results of T- and X-joints are not directly comparable in terms of the nominal stress system. The

angular distortion can be considered when the HS stress system is applied. Since secondary bending occurred only in the T-joints, their fatigue strength improves notably with respect to the X-joints, Fig. 6b. When fixed $m = 3$ is applied, the test results predict a 35% higher FAT_{HS} for the T-joints. As stated, the symmetric case generates a greater notch effect than the asymmetric case, and consequently, the higher fatigue strength of asymmetric T-joints in the HS stress system was presupposed.

Literature widely provides SCF formulae for fillet welded transverse attachment joints determined by means of boundary or finite element methods.[7,15,16] However, the found formulae have generally geometrical limitations or are not fully applicable to bending. To accomplish consistent and reliable results, it was reasonable to evaluate the SCF by using FEA. In the ENS approach, *S-N* curves were determined by using actual notch radius $\rho = 0$ for the worst case when the effective SCF k_f is equal to k_t ($r = 1$ mm).[17,18] This concept was utilized when the test results were adapted to the notch stress system. Since both nominal and effective throat thicknesses varied slightly along the weld, the mean values of the measured geometrical data were used. In the analyses, $a_{mean} = 5.2$ mm, effective throat thickness $a_{eff} = 5.8$ mm, flank angle $\theta = 45°$ and notch radius $r = 1$ mm were applied. The derived SCFs for such a geometry are presented in Table 4. The used element models are presented in the next Section, Fig. 9.

Table 4 Derived SCFs for the test specimens.

Loading/Joint type	Asymmetric T-joint	Symmetric X-joint
Tension	1.854	2.325
Bending	2.064	1.791

The membrane and bending stress components of HS stress in the T-joints were separated and multiplied by effective SCFs. In Fig. 6c, the test data of tensile loaded joints are plotted in terms of the ENS method. Since a higher notch effect occurs in the X-joints subjected to axial loading, the notch stress system seems to equalize the results to a common *S-N* curve.

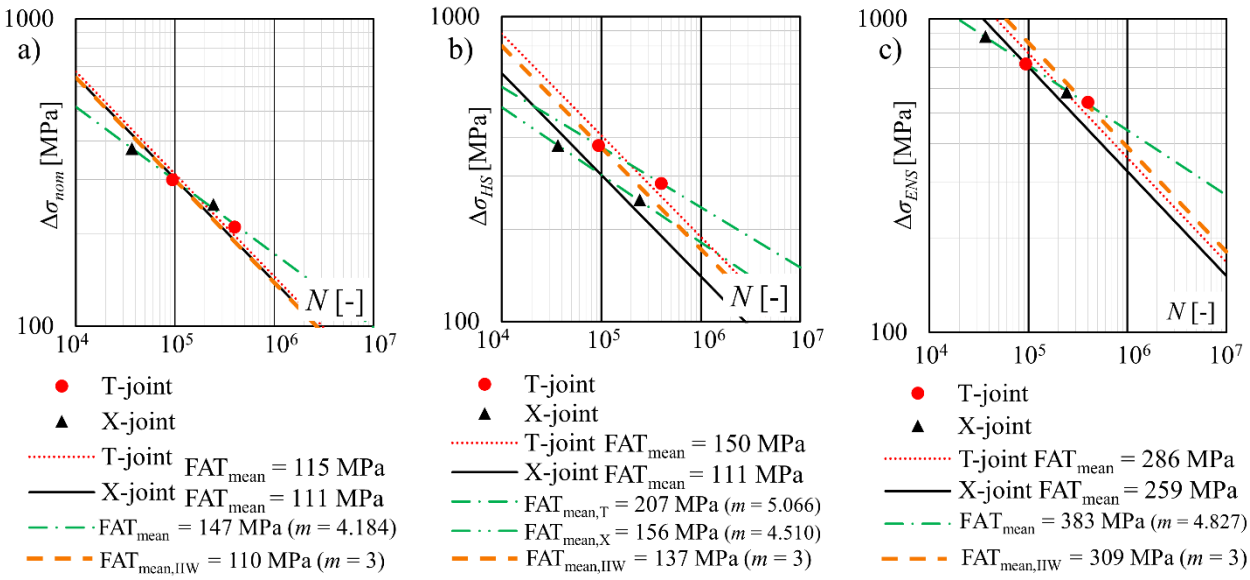

Fig. 6 Plotted test data and evaluated *S-N* curves for tensile loaded joints in terms of (a) nominal stress, (b) HS stress and (c) ENS systems. In nominal stress and ENS systems, FAT_{mean} represents a common *S-N* curve for both joint types.

In the joints subjected to pure bending (DOB = 1), the secondary bending stress did not occur, and hence, the nominal stresses are equal to HS stresses, Fig. 7a. The test results advocate that the increasing DOB consistently gives a higher fatigue strength for both joint types. In the nominal stress system, the mean fatigue strength (m = 3) of DOB = 1, compared to tensile loading, is 57% and 47% higher in the T- and X-joints, respectively. In terms of the HS stress system, the difference in the fatigue strengths between tensile and bending loaded asymmetric T-joints decreases owing to the secondary bending stress but it is still notable. When comparing the test results of bending loaded joints, the nominal and HS stress systems predict that the fatigue strength of T-joints is only slightly higher with respect to X-joints. However, the notch effect of asymmetric T-joints is more severe, and thus, it raises the ENS range and unexpectedly distinguishes the data points in terms of the ENS system, Fig. 7b.

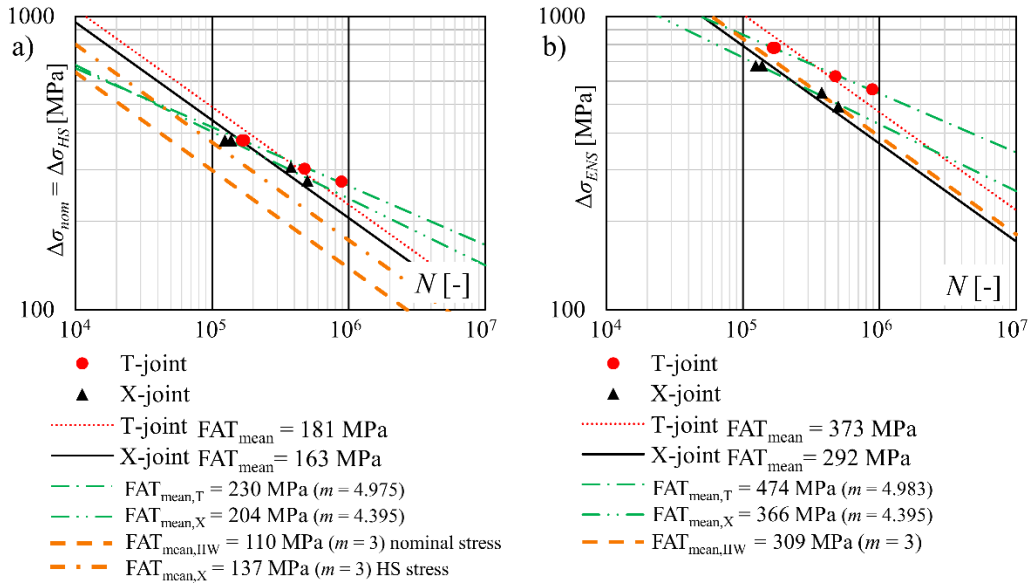

Fig. 7 Plotted test data and evaluated *S-N* curves for bending loaded joints in terms of (a) nominal and HS stress and (b) ENS systems.

A difference between the tensile and bending loaded joints can be recognized also in the final ruptures of the test specimens, Fig. 8. When the crack has propagated across the plate width, the section modulus of the base plate has a quadratic dependency on the unbroken height. Because of this, under bending loading, the nominal stress at the crack tip increases more than under tensile loading, in which the stress is directly proportional to the unbroken height. Consequently, in the bending loaded joints (IDs 1–4), the maximum nominal stress of the specimen exceeded the yield strength of the material and a ductile failure occurred. Respectively, in the tensile loaded joints (IDs 5–6), the maximum SIF exceeded the fracture toughness of the material and the representative block-shaped fracture surface of the brittle failure can be seen at the edges of the fatigue cracks.

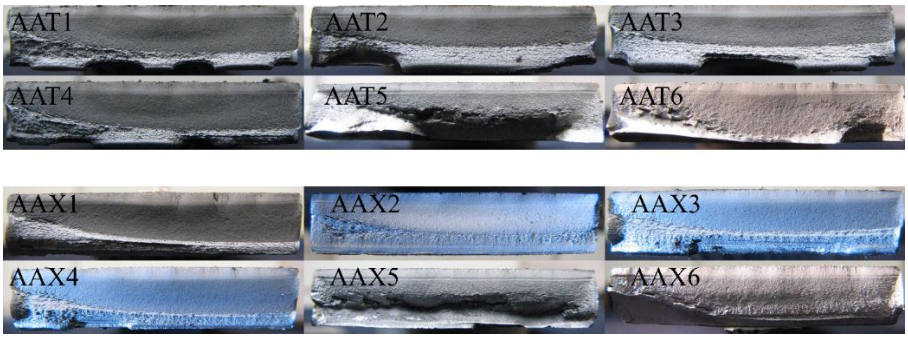

Fig. 8 Final ruptures of the test specimens. Specimen IDs 1-4 were subjected to bending and IDs 5-6 to tension.

FATIGUE ASSESSMENT

Finite element models

FEAs were carried out to compare the computational fatigue assessment methods to the test results. For the transverse attachment joints, 2D plane strain models were used. Femap with NX Nastran software was used in the stress based approaches and crack growth simulations were performed by using the FRANC2D V4 program. Half models with symmetry constraints were utilized in the analyses. SCFs were determined for the evaluation of the test results in terms of the ENS method, Fig. 9a. An extremely fine and quadrilateral mesh with an absolute size of 0.05 mm (r/20, 120 elements over 360°) was applied to the weld toe, while IIW recommends a mesh size of $\leq r/4$ for the elements with a quadratic displacement order.[19] Baumgartner *et al.*[20] showed that the notch stress converges extremely well when the number of elements over 360° exceeds 50.

In the tensile loaded T-joints (AAT5 and AAT6), the k_m factors were determined by means of the HS stress models, Fig 9b. Geometrically non-linear analyses were performed by taking the measured angular distortion and test loading into account. The linear surface extrapolation (LSE) and through thickness at weld toe (TTWT) methods[21] were adopted in the evaluation of $k_{m,FEA,SL}$ factors. Table 5 presents the defined factors which agree well with the analytically formed values in Table 3. Nevertheless, the angular distortions were actually lower than the shape laser measurements predicted, and thus, the angular distortions were conversely re-calculated by placing $k_{m,SG}$, Table 3, in Eq. (1) without considering the tanh(β) correction. Consequently, the initial straightening due to the clamping was taken into account in the FE models. The used procedure gives an approximation of the actual angular misalignment. To take the clamping into account more comprehensively, separate FEAs, in which the clamping is the first load step before the axial loading, should be conducted. However, these analyses were not employed in this study. The evaluated angular distortions, α_{SG}, are presented in Table 5. These values were utilized in the HS models in which linear analyses were carried out. In that case, the $k_{m,FEA,SG}$ factors, Table 5, corresponded well with the $k_{m,SG}$ presented in Table 3. It can also be seen that $\sigma_{0.4t}$ equals approximately to the HS stress, i.e. the extrapolation does not have a major influence on the evaluated HS stress. The defined angular distortions, α_{SG}, were also applied in the ENS and LEFM models with linear analyses. Crack growth was determined based on the maximum tangential stress criterion and the SIFs of the opening mode I and sliding mode II (K_I and K_{II}) were calculated. In the analyses, K_I and K_{II} were computed by using the inbuilt J-integral approach introduced by Dodds *et al.*[22].

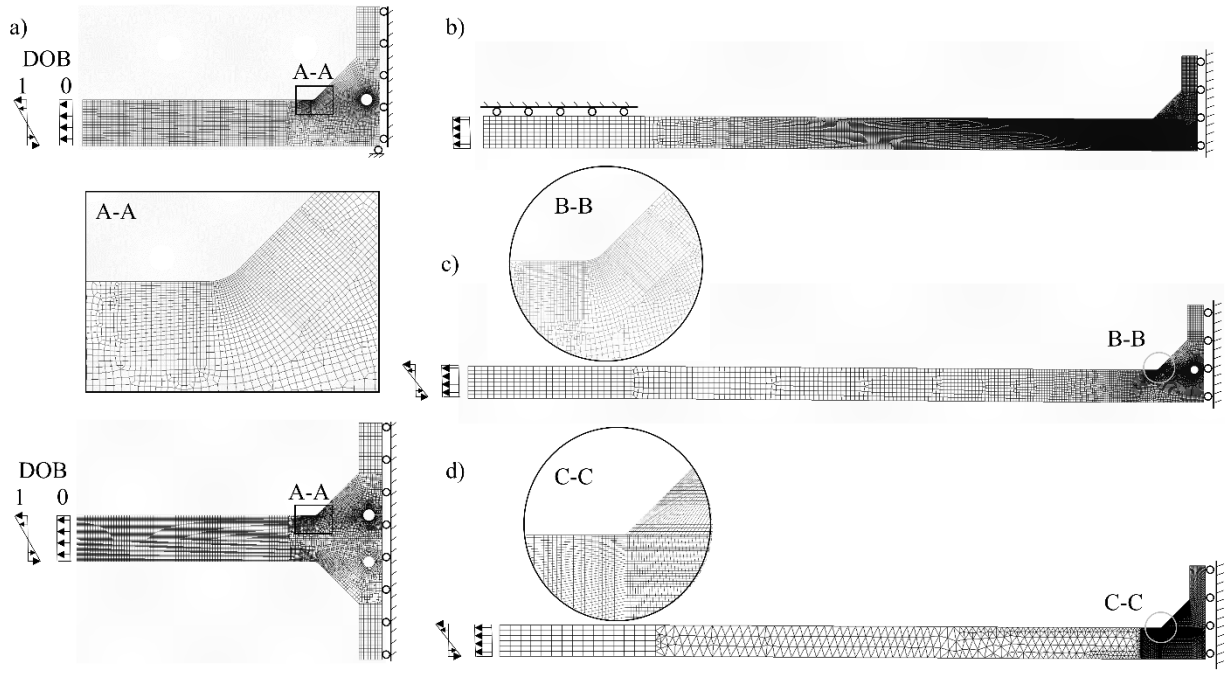

Fig. 9 FEA models: (a) the evaluation of the SCF, (b) the HS stress method, (c) the ENS method and (d) LEFM.

Table 5 k_m factors of the tensile loaded T-joints evaluated on the basis of FEA

ID	$k_{m,FEA,SL}$ [-]				$k_{m,FEA,SG}$ [-]				
	$\sigma_{0.4t}/\sigma_{nom}$	$\sigma_{1.0t}/\sigma_{nom}$	LSE	TTWT	α_{SG} [10^{-3} rad]	$\sigma_{0.4t}/\sigma_{nom}$	$\sigma_{1.0t}/\sigma_{nom}$	LSE	TTWT
AAT5	1.378	1.339	1.40	1.40	10.7	1.277	1.254	1.29	1.29
AAT6	1.481	1.433	1.51	1.51	14.4	1.365	1.336	1.39	1.38

The mean values of the approaches' coefficients were used in the fatigue assessment. In the design *S-N* curves, the deviation of the test data is covered and the computation of FAT_{char} is based on the survival probability of 97.7%, i.e. mean minus two standard deviation. In that case, the safety factor is j_σ = 1.37. The computed mean fatigue strengths, FAT_{mean}, for the stress based approaches are presented in Table 6.[4,17,18]

Table 6 Computed mean fatigue strengths of the stress based approaches.

Approach	FAT_{char} [MPa]	FAT_{mean} [MPa]
Nominal	80	110
HS	100	137
ENS	225	309

In LEFM, the fatigue life was assessed by applying the generally accepted Paris' crack propagation law

$$\frac{\mathrm{d}a}{\mathrm{d}N} = C \cdot \Delta K^m \,, \tag{8}$$

where da/dN is the crack propagation rate, C the crack propagation coefficient, ΔK the SIF range and m the slope of Paris' law.[23] Finally, by separating the variables of Eq. (8) and integrating from the initial crack length a_i to the final crack length a_f, the fatigue life can be expressed as follows:

$$N_f = \int_{a_i}^{a_f} \frac{\mathrm{d}a}{C \cdot \Delta K^m} \,. \tag{9}$$

$C_{mean} = 1.7 \cdot 10^{-13}$ (da/dN in mm/cycle and ΔK in MPa $\cdot$ mm$^{0.5}$) can be estimated when $C_{char} = 3.0 \cdot 10^{-13}$ is valid.[24] The use of the engineering crack propagation coefficients, e.g. given in BS7910[25], would lead approximately equal fatigue life estimations. Furthermore, $a_i = 0.05$ mm was applied since it has been demonstrated to agree with the test results reasonably well.[26, 27] Fatigue life estimation is not sensitive to the final crack size but $a_f = 6$ mm was chosen based on the final ruptures of the test specimens.

Results

Fig. 10 presents the calculated mean fatigue lives in comparison with the test results. In the tensile loaded joints, Fig. 10a, the nominal and HS stress methods agree well with the test results. However, the data points of the HS stress method do not fit on the same curve, as expected. The ENS method seems to be non-conservative, particularly in the low-cycle regime. Respectively, LEFM is overly conservative and the assessed fatigue lives are below the characteristic fatigue lives. Test results demonstrated distinctly that the increasing DOB gives a higher fatigue strength. For that reason, the fatigue life estimations, Fig. 10b, are more conservative than in the tensile load case. Fatigue strengths assessed by the ENS method agree well with the test results, but the estimations deviate around the mean curve. The nominal and HS stress methods are more conservative than the ENS method, but the deviation is lower. LEFM is even more conservative than in the tensile load case and does not give proper estimations of fatigue life.

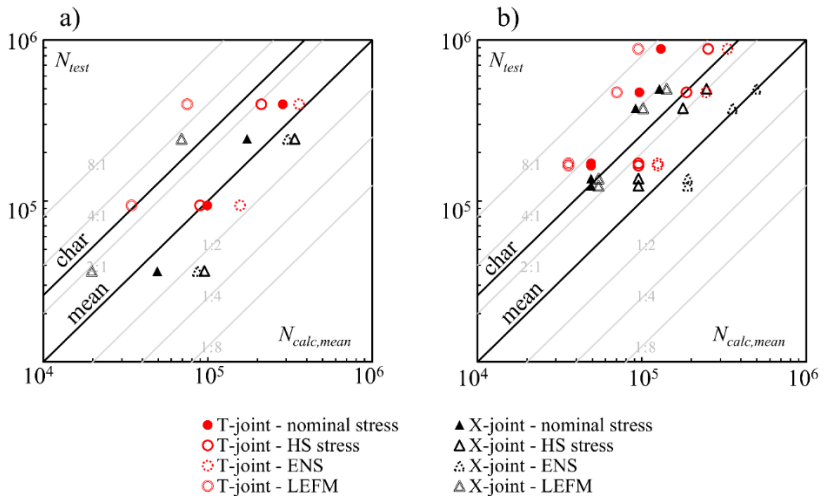

Fig. 10 Calculated fatigue lives compared to the test results: (a) tensile and (b) bending loaded joints.

As stated, LEFM gives overly conservative estimations of fatigue life. Most likely, the most significant reason for this is the crack initiation time, which stands out particularly in UHSSs with respect to conventional mild steels.[28] Fatigue life N_f is composed of crack initiation time N_i and crack propagation time N_{cp}, which are summarized for each test in Table 3. The crack initiation time is emphasized particularly in the high-cycle regime that can be seen also from the evaluated *S*-*N* curves in which $m = 3$ was overly steep. The accurate monitoring of crack initiation and crack propagation times is complex, but it is possible by examining the changes in the measurements of the strain gage which was inserted into every specimen. As long as crack initiation occurs, the stress remains constant at the strain gage position. Once initial cracks have developed, stress variation at the surface of the specimen decreased, which was monitored, Fig. 11a. If the crack does not initiate opposite the strain gage, the precise time of crack initiation cannot be determined, but this method gives a reasonable estimation. As shown in Fig. 8, the fatigue cracks initiated in the continuous part of the welds although not in the middle of the welds. However, the effect of the crack location on the evaluation of crack initiation time was not considered in this study. In this study, the crack propagation was considered to have been started when approximately a 5% reduction in the strain range occurred. Fig. 11b shows the measured crack propagation time divided by the calculated one.

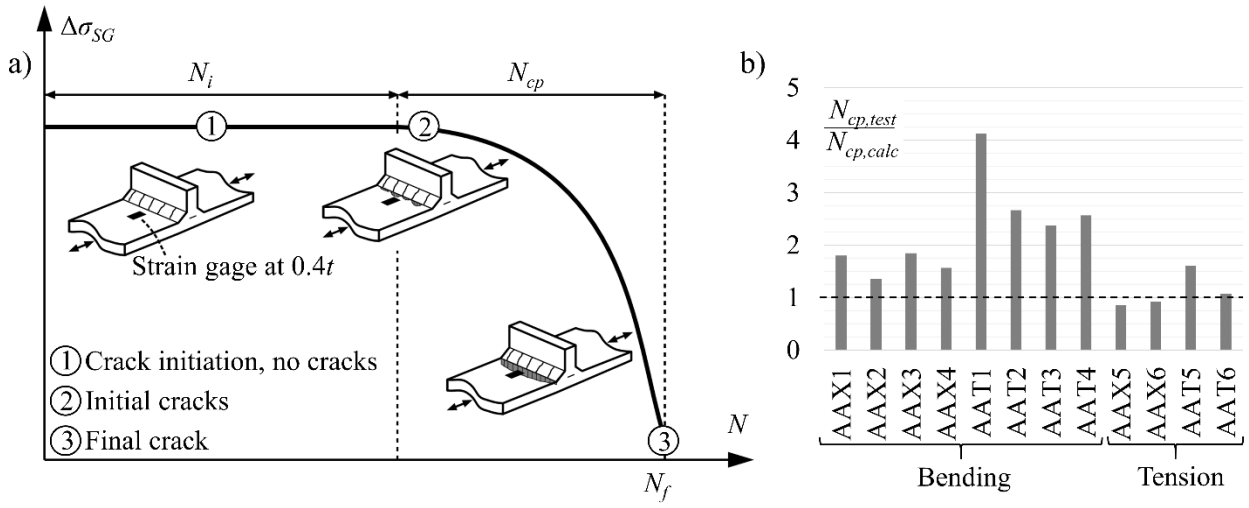

Fig. 11 (a) Principle of the evaluation of crack propagation and initiation times and (b) obtained results.

Fig. 11b shows that in the bending loaded joints, 2D LEFM distinctly underestimates the crack propagation time. Furthermore, the tested T-joints seemed to have consistently longer crack propagation times than LEFM estimated. Respectively, in the tensile load case, the calculated crack propagation times have good agreement with the test results and only specimen AAT5 gave an anomalous result.

DISCUSSION

Experimental fatigue tests and FEA for transverse non-load carrying attachment joints were carried out to investigate the effect of the loading type and geometrical symmetry on the fatigue strength. Under tensile loading, both fatigue tests and FEAs showed that the fatigue strength of asymmetric T-joints is higher than the corresponding symmetric X-joints. In the fatigue tests, the nominal stress system apparently fit the data points on the common *S*-*N* curve, Fig. 6a, due to higher angular distortion in the T-joints, but if the angular distortion of T- and X-joints had been equal, the fatigue strength of the T-joints would have been higher compared to the X-joints, most likely.

In the fatigue tests, bending loading improved the fatigue capacity of both T- and X-joints, and higher fatigue strengths were obtained compared to the tensile load case, Fig. 7. In the symmetric X-joints, this was expected since bending stress develops a gentler notch effect than membrane loading. Respectively, in the asymmetric T-joints, bending produces more severe stress concentration, Table 4, at the weld toe, and hence, a definite improvement in fatigue strength was unexpected. Owing to the mounting and clamping of tensile loaded T-joint specimens, the mean

stress level increased, which decreases the fatigue strength but does not solely explain the difference between the tensile and bending test results. 2D LEFM showed the beneficial effect of bending, which was not as great as the test results predicted. Table 7 summarizes the effect of the loading type and geometrical symmetry on the fatigue strength of the tested specimens.

Table 7 Fatigue strength ratios of test results and fatigue assessment. The ratios are determined by using the fixed $m = 3$ slope and FAT_{mean}.

	Experimental			Fatigue assessment			
Ratio	Nominal stress	HS stress	ENS	Nominal stress	HS stress	ENS	LEFM
$q_{geom,m}$	1.04	1.35	1.10	0.75*	1.00	1.24	1.23
$q_{geom,b}$	1.11	1.11	1.28	1.00	1.00	0.87	0.87
$q_{load,asym}$	0.64	0.83	0.77	0.75*	1.00	1.09	1.00
$q_{load,sym}$	0.68	0.68	0.87	1.00	1.00	0.77	0.71

Compressive residual stresses were measured at the weld toes although the specimens were in ASW condition. This might be one explanation for the higher FAT values obtained in the bending loaded joints. It was noticed also by Ottersböck *et al.*[12] that the fatigue strength of bending loaded joints improves significantly when high-frequency mechanical impact post-weld treatment is applied when high compressive residual stresses are achieved. This might be explained by the combined effect of residual stress and the stress gradient. Nevertheless, the effect of residual stresses on the fatigue resistance of bending loaded joints would require more comprehensive analyses and measurements and is not in the scope of this study.

The experimental tests and FEAs were carried out only for small-scale specimens. Consequently, only somewhat load-controlled behavior was studied in this paper. When the effect of the loading type and geometrical symmetry on the fatigue resistance is applied in the welded structures, the behavior of the real structure, i.e. forced displacements and local constraints, must be considered. In the discussed studies[1, 3, 9, 10, 12], the comparisons have been made by the nominal stress system in which secondary effects cannot be considered comprehensively.

CONCLUSIONS

In this study, the effect of symmetry and loading type on the fatigue strength of non-load carrying joints was investigated by conducting experimental fatigue tests and finite element analyses. According to the obtained results, the following conclusions can be drawn:

- The fatigue strength of asymmetric T-joints is higher than the corresponding symmetric X-joints under tensile loading on the basis of experimental tests and FEA. The symmetry of the joint increases the notch effect at weld toe, leading to lower fatigue resistance. This aspect is completely neglected in the existing codes.
- Fatigue assessment methods exhibit a slight loss of fatigue strength in the non-load carrying asymmetric T-joints when external loading is bending. In the symmetric X-joints, the notch effect decreases under bending loading and higher fatigue strengths are obtained.
- Test results showed an improvement of fatigue strength in both bending loaded asymmetric T-joints and symmetric X-joints. This study advocates the complexity of bending in the fatigue assessment of welded joints.

To establish unambiguous statements about the effect of bending on the fatigue resistance of welded joints, further tests and analyses will be needed in the future. For instance, tests should be carried out for welds of various qualities, and thus, different residual stress states and weld toe geometries can be considered. Additionally, different joint types should be observed. Further analyses and fatigue tests would also clarify the mechanical background of the different fatigue behavior of asymmetric T-joints and symmetric X-joints.

ACKNOWLEDGEMENTS

This study was carried out as a part of the Breakthrough Steels and Applications (BSA) program. The authors wish to thank SSAB and FIMECC Ltd. as well as the Finnish Funding Agency for Innovation (TEKES) for their funding during this project.

REFERENCES

1. Maddox S J (2015). Allowance for bending in fatigue design rules for welded joints. IIW-doc. XIII-2580-15.
2. Kang S W, Kim W S, Paik Y M (2002) Fatigue strength of fillet welded steel structure under out-of-plane bending load. *Int. J. KWS*, **2**. 33–37.
3. Xiao Z G, Chen T, Zhao X L (2012). Fatigue strength evaluation of transverse fillet welded joints subjected to bending loads. *Int. J. Fatigue*, **38**. 57–64.

4. Hobbacher A (2014). Recommendations for fatigue design of welded joints and components. IIW-doc. XIII-2460-13/XV-1440-13.
5. EN 1993-1-9 (2005). Eurocode 3: Design of Steel Structures. Part 1-9: Fatigue. Brussels: European Committee for Standardization.
6. DNVGL-RP-C203 (2014). Fatigue design of offshore steel structures. DNV GL AS.
7. Iida K, Uemura, T (1996). Stress concentration factor formulae widely used in Japan. *Fatigue Fract. Engng Mater. Struct.*, **19**. 779–786.
8. Lie S T., Vipin S P, Li T (2015). New weld toe magnification factors for semi-elliptical cracks in double-sided T-butt joints and cruciform X-joints. *Int. J. Fatigue*, **80**. 178–191.
9. Kim I T, Jeong Y S (2013). Fatigue strength improvement of welded joints by blast cleaning for subsequent painting. *Int. J. Steel Struct.*, **13**. 11–20.
10. Baik B, Yamada K, Ishikawa T (2011). Fatigue crack propagation analysis for welded joint subjected to bending. *Int. J. Fatigue*, **33**. 746–758.
11. Lotsberg I, Sigurdsson G (2006). Hot spot stress S-N curve for fatigue analysis of plated structures. *J. Offshore Mechanics and Arctic Engng*, **128**. 330-336.
12. Ottersböck M, Leitner M, Stoschka M (2015). Effect of loading type on welded and HFMI-treated T-joints. IIW-doc. XIII-2584-15.
13. EN 1993-1-8 (2005). Eurocode 3: Design of Steel Structures. Part 1-9: Design of joints. Brussels: European Committee for Standardization.
14. Takeuchi K (2012). Locations of strain gauges for fatigue analysis of welded joints (2). *Welding Int.*, **26**. 655–664.
15. Brennan F P, Peleties P, Hellier A K (2000). Predicting weld toe stress concentration factors for T and skewed T-joint plate connections. *Int. J. Fatigue*, **22**. 573–584.
16. Pluvinage G (2003). *Fracture and fatigue emanating from stress concentrators*. Kluwer Academic Publishers, Dordrecht, Holland.
17. Sonsino C M, Fricke W, de Bruyne F, Hoppe A, Ahmadi A, Zhang G (2012). Notch stress concepts for the fatigue of welded joints – background and applications. *Int. J. Fatigue*, **34**. 2–16.
18. Radaj D, Sonsino C M, Fricke W (2006). *Fatigue assessment of welded joints by local approaches.* Woodhead Publishing Ltd, Cambridge, UK.
19. Fricke W (2012). *IIW recommendations for the fatigue assessment by notch stress analysis for welded structures*. Woodhead Publishing Ltd, Cambridge, UK.
20. Baumgartner J, Bruder T (2013). An efficient meshing approach for the calculation of notch stresses. *Welding in the World*, **57**. 137–145.
21. Poutiainen I, Tanskanen P, Marquis G (2004). Finite element methods for structural hot spot stress determination – a comparison of procedures. *Int. J. Fatigue*, **26**. 1147–1157.
22. Dodds R H, Vargas P M (1988). *Numerical evaluation of domain and contour integral for non-linear fracture mechanics: formulation and implementation aspects*. Report UILU-ENG-88-2006. University of Illinois at Urbana-Champaign, Department of Mechanical Engineering.
23. Dowling N E (1999). *Mechanical behavior of materials*. 2nd edition. Prentice-Hall, New Jersey, USA.
24. Nykänen T, Li X, Björk T, Marquis G (2005). A parametric fracture mechanics study of welded joints with toe cracks and lack of penetration. *Engng Fract. Mech.*, **72**. 1580–1609.
25. BS7910 (2013). Guide to methods for assessing the acceptability of flaws in metallic structures. London: British Standards Institution.
26. Nykänen T, Marquis G, Björk T (2007). Fatigue analysis of non-load-carrying fillet welded cruciform joints. In: Marquis G, Samuelsson J, Agerskov H, Haagensen P J (editors). *Proceedings of the international symposium on integrated design and manufacturing of welded structures*. March 13–14, 2007, Eskiltstuna, Sweden.
27. Nykänen T, Marquis G, Björk T (2009). A simplified fatigue assessment method for high quality welded cruciform joints. *Int. J. Fatigue*, **31**. 79–87.
28. Sperle J O (2008). Influence of parent metal strength on the fatigue strength of parent material with machined and thermally cut edges. *Weld World*, **52**. 79–92.